Ion–water hydrogen-bond switching observed with 2D IR vibrational echo chemical exchange spectroscopy

David E. Moilanen, Daryl Wong, Daniel E. Rosenfeld, Emily E. Fenn, and M. D. Fayer[1]

Department of Chemistry, Stanford University, Stanford, CA 94305

Contributed by M. D. Fayer, November 12, 2008 (sent for review November 8, 2008)

The exchange of water hydroxyl hydrogen bonds between anions and water oxygens is observed directly with ultrafast 2D IR vibrational echo chemical exchange spectroscopy (CES). The OD hydroxyl stretch of dilute HOD in H_2O in concentrated (5.5 M) aqueous solutions of sodium tetrafluoroborate ($NaBF_4$) displays a spectrum with a broad water-like band (hydroxyl bound to water oxygen) and a resolved, blue shifted band (hydroxyl bound to BF_4^-). At short time (200 fs), the 2D IR vibrational echo spectrum has 4 peaks, 2 on the diagonal and 2 off-diagonal. The 2 diagonal peaks are the 0–1 transitions of the water-like band and the hydroxyl-anion band. Vibrational echo emissions at the 1–2 transition frequencies give rise to 2 off-diagonal peaks. On a picosecond time scale, additional off-diagonal peaks grow in. These new peaks arise from chemical exchange between water hydroxyls bound to anions and hydroxyls bound to water oxygens. The growth of the chemical exchange peaks yields the time dependence of anion–water hydroxyl hydrogen bond switching under thermal equilibrium conditions as $T_{aw} = 7 \pm 1$ ps. Pump-probe measurements of the orientational relaxation rates and vibrational lifetimes are used in the CES data analysis. The pump-probe measurements are shown to have the correct functional form for a system undergoing exchange.

2D IR spectroscopy | hydration of ions | hydrogen bond dynamics | ion hydrogen bonds chemical exchange | ionic solutions

Water interacting with ions occurs in a wide variety of systems ranging from ocean salt water to water interacting with charged amino acids at the surfaces of proteins (1). The properties of pure liquid water are determined by the nature of its hydrogen bond network. A water molecule can have as many as 4 hydrogen bonds with other water molecules, forming an approximately tetrahedral structure. The pure water hydrogen bond network is constantly evolving with a range of time scales from tens of femtoseconds to picoseconds (2–5). Hydrogen bonds are continually forming and breaking through concerted hydrogen bond rearrangements (6). These dynamical processes can be observed on the time scale they occur in considerable detail by using ultrafast infrared spectroscopy. Measurements of spectral diffusion, described in terms of the frequency–frequency correlation function (FFCF), by using ultrafast 2D IR vibrational echo spectroscopy (3, 7, 8) as well as other ultrafast IR techniques (4, 5) have determined the multiple time scales for the hydrogen bond dynamics. The slowest time component of the FFCF (1.7 ps) is associated with the randomization of the hydrogen bond network through concerted hydrogen bond rearrangements. The orientational relaxation time of pure water (2.6 ps) (2, 5) is also assigned to concerted hydrogen bond rearrangement via jump reorientation (6).

In aqueous salt solutions the structure of water is modified in the vicinity of the ions as the water oxygens preferentially solvate the cations and the water hydroxyls solvate the anions (9, 10). The structures of the hydration shells around individual ions, charged groups of large molecules, or charged amino acids on the surfaces of proteins are determined by ion–dipole interactions between water molecules and the charged group (11, 12). These interactions will influence both the structure and dynamics of water in the proximity of ions.

In pure water, the hydroxyl stretching IR absorption band is very broad because of the distribution of strengths and numbers of hydrogen bonds (13, 14). When salt is added, hydrogen bonding to the ions causes shifts of the hydroxyl stretch frequency (15–17). The stretching frequency is sensitive primarily to the type of anion and, to a lesser extent, the cation. Addition of NaCl, NaBr, and NaI cause blue shifts of the spectrum that increase as the anion becomes bigger (17). For these salts, the spectra are broad and the shifts are not large. The hydroxyl–anion spectra overlap substantially with the spectrum of hydroxyls bound to water oxygens so that the hydroxyl–anion spectra are not resolved from the hydroxyl–water oxygen spectrum.

Here, we present the results of ultrafast 2D IR vibrational echo chemical exchange experiments on an aqueous solution of the anion BF_4^- from the salt $NaBF_4$. For this anion, the stretch spectrum of hydroxyls bound to BF_4^- is substantially shifted to the blue, and the band is relatively narrow (16). The hydroxyl–anion peak is readily observable on the high-frequency side of the broad hydroxyl–oxygen band (see Fig. 1). The observed splitting of the hydroxyl-anion peak from the hydroxyl–water peak makes the experiments discussed here possible.

Ionic hydration and the dynamics of water in salt solutions have been studied extensively by NMR (10, 18), neutron diffraction (19), computer simulations (20–22), and infrared spectroscopy (8, 15, 17, 23). A great deal is known about the structure of ionic solvation shells from diffraction experiments. However, unraveling the dynamics of the solvation shell and the back and forth exchange of waters hydrogen bonded to ions and to water molecules is a much more difficult experimental problem.

A number of studies using ultrafast infrared experiments performed on the water hydroxyl stretching mode have been directed at determining the influence of salts on water dynamics and the rates of hydrogen bond switching between water and anions (8, 24). These experiments (8, 24) and related theory (20–22) have provided insights into water–ion dynamics. However, unambiguous experimental determination of the hydrogen bond switching rate is difficult because the 2 types of hydroxyls are not usually spectroscopically resolved. Below, we report the direct observation of exchange of hydroxyl hydrogen bonds between water and BF_4^- anions using ultrafast 2D IR vibrational echo chemical exchange spectroscopy (25).

Author contributions: D.E.M., D.E.R., and M.D.F. designed research; D.E.M., D.W., D.E.R., E.E.F., and M.D.F. performed research; D.W. contributed new reagents/analytic tools; D.E.M., D.W., D.E.R., E.E.F., and M.D.F. analyzed data; and D.E.M. and M.D.F. wrote the paper.

The authors declare no conflict of interest.

[1]To whom correspondence should be addressed. E-mail: fayer@stanford.edu.

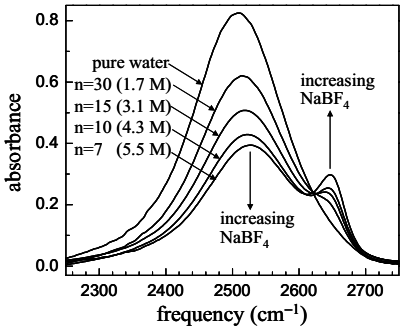

Fig. 1. Infrared absorption spectra of the OD stretch of 5% HOD in H_2O for various concentrations of $NaBF_4$ and pure water.

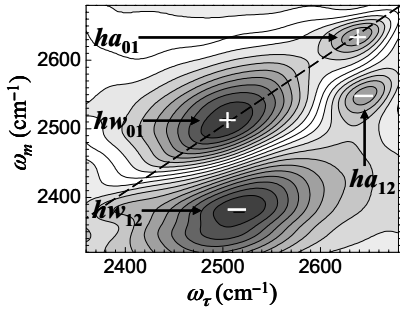

Fig. 2. The 2D IR vibrational echo spectrum of the $n = 7$ solution of $NaBF_4$ at $T_w = 200$ fs, a time short compared with chemical exchange. Positive going peaks are marked by + and negative going peaks are marked by −.

Chemical exchange occurs when 2 species in equilibrium interconvert without changing the overall number of either species. Chemical exchange spectroscopy (CES) has been developed recently (25–29) and applied to the formation and dissociation dynamics of organic solute–solvent complexes (25, 26, 30) the rate of isomerization around a carbon–carbon single bond (29) and the switching between well-defined protein structural substates (31).

Chemical exchange between 2 species has a well-defined effect on the 2D IR vibrational echo spectrum. At times short compared with the exchange time, the peaks in the IR absorption spectrum corresponding to the 2 species appear as 2 bands going in the positive direction on the diagonal of the 2D spectrum. In addition, there are 2 off-diagonal bands going in the negative direction that arise from vibrational echo emission at the $v = 1$ to $v = 2$ (1–2) transition frequencies of each diagonal peak. The 1–2 peaks are shifted to lower frequency along the vibrational echo emission (vertical) axis of the 2D spectrum by the anharmonicities of the 2 transitions that give rise to the diagonal peaks. At longer times, 4 additional off-diagonal peaks grow in because of chemical exchange. The time-dependent growth of these exchange peaks provides a direct measurement of the chemical exchange rate. A detailed discussion of the chemical exchange process has been given by Kwak *et al.* (27).

At early delay times in the experiments on $NaBF_4$ solutions presented below, the 2D IR CES spectrum only displays well-resolved hydroxyl–water (*hw*) and hydroxyl–anion (*ha*) bands. The *hw* signifies hydroxyls hydrogen bonded to the oxygen atoms of water molecules; *ha* signifies hydroxyls hydrogen bonded to the BF_4^- anions. As time increases, off-diagonal peaks grow in because of hydrogen bond rearrangements that cause *ha* to change into *hw* and vice versa. The exchange dynamics are extracted from the time-dependent growth of these off-diagonal peaks when the effects of the vibrational lifetimes and orientational relaxation of the 2 species are included in the analysis. The vibrational lifetimes and orientational relaxation times are measured with polarization-selective IR pump-probe experiments. The *ha*/*hw* equilibrium constant and the ratio of the transition dipoles of *hw* and *ha* stretching modes are found from a combination of the linear IR absorption spectrum and the 2D IR spectrum. The equilibrium constant obtained here is consistent with one obtained by X-ray diffraction (32). For the 5.5 M $NaBF_4$ solution (7 water molecules per $NaBF_4$, or 14 hydroxyls per BF_4^- anion) studied here, the equilibrium constant for hydroxyl–ion/hydroxyl–water (*ha*/*hw*) is 0.3, and the $ha \rightarrow hw$ exchange time is 7 ± 1 ps.

Results and Discussion

The OD hydroxyl stretch of dilute HOD in H_2O is studied rather than pure H_2O or D_2O to eliminate vibrational excitation transfer (33, 34). Vibrational excitation transfer changes the spatial location of the excitation causing the decay of the transition dipole anisotropy (35), which interferes with orientational relaxation measurements and will artificially contribute to chemical exchange. MD simulations have shown that dilute HOD in H_2O does not change the behavior of water and that observations of the OD hydroxyl stretch report on the dynamics and local environment of water (36).

Details of 2D-IR vibrational echoes and CES experiments have been presented previously (25, 27, 29, 37). Briefly, 3 IR pulses tuned to the frequency of the OD stretch in the water/$NaBF_4$ solution (≈2,550 cm^{-1}) are crossed in the sample. Because the pulses are short, they have a broad bandwidth that makes it possible to simultaneously excite the vibrational transitions of both the *hw* and *ha* species. The first laser pulse "labels" the initial structures of the species by defining their initial frequencies, ω_τ (horizontal axis in Figs. 2 and 3). The second pulse ends the first time period τ and starts clocking the reaction time period T_w during which the labeled species undergo $hw \leftrightarrow ha$ switching (chemical exchange), as well as orientational relaxation and vibrational population relaxation. The third pulse ends the population dynamics period of length T_w and begins a third period of length $\leq\tau$, which ends with the emission of the vibrational echo pulse of frequencies ω_m (vertical

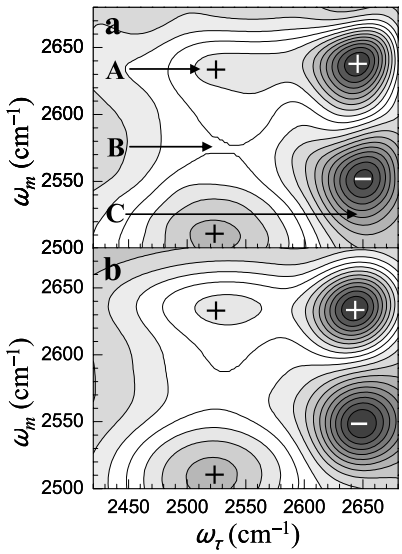

Fig. 3. The 2D IR vibrational echo spectrum (*a*) and calculated spectrum (*b*) of the $n = 7$ solution of $NaBF_4$ at $T_w = 4$ ps. Peaks going in the positive direction are marked by +, and peaks going in the negative direction are marked by −. By 4 ps, additional peaks labeled A, B, and C have grown in because of chemical exchange. The data and calculated spectrum agrees well.

axis in Figs. 2 and 3). The vibrational echo signal reads out information about the final structures of all labeled species by their frequencies ω_m.

There are 2 types of time periods in the experiment. The times between pulses 1 and 2 and between pulse 3 and the vibrational echo pulse are called coherence periods. During these periods, the OD vibrations are in coherent superpositions of 2 vibrational states. Fast frequency fluctuations of the vibrational oscillators induced by fast structural fluctuations of the system cause dynamic dephasing, which is one contribution to the line shapes in the conventional absorption spectrum. During the period T_w between pulses 2 and 3, called the population period, an oscillator is in a vibrational eigenstate. Slower structural fluctuations of the system cause the OD frequency to evolve in time. This time evolution of the frequency, termed spectral diffusion, contributes to the 2D line shapes. As discussed in the Introduction, during the time period T_w, chemical exchange causes off-diagonal peaks to grow in.

There are several factors that contribute to the time dependence of the 2D IR spectra. Vibrational population relaxation and orientational relaxation cause all of the peaks to decay. Whereas population relaxation will eventually cause all peaks to decay to zero, orientational relaxation reduces the amplitudes of all of the peaks but not to zero. Spectral diffusion causes all peaks to change in shape but preserves the peak volumes. Chemical exchange causes the diagonal peaks to partially decay. Only the off-diagonal chemical exchange peaks grow in amplitude. By determining the time dependence of the peak volumes, spectral diffusion is eliminated from the determination of the chemical exchange rate. The population relaxation and orientational relaxation are measured by polarization-selective pump-probe experiments and used in the data analysis as discussed below (27).

Analysis of the data following the methods of Kwak *et al.* (27) yields the exchange rate. The number of $hw \rightarrow ha$ exchanges is equal to the number of $ha \rightarrow hw$ exchanges because the system is in equilibrium. To determine the exchange times, it is necessary to know the equilibrium constant, which is the ratio R of hydroxyls bound to anions to hydroxyls bound to water. X-ray diffraction studies of $NaBF_4$ at almost the same concentration used here (7 waters per $NaBF_4$) indicate that $\approx$4 water molecules (4 hydroxyls of 14) hydrate a BF_4^- (32).

The equilibrium constant R can also be determined by a comparison of the linear IR spectrum to the 2D IR spectrum. In the IR absorption experiments (see Fig. 1), the areas of the *hw* band and the *ha* band were determined. If the transition dipoles, μ_{hw} and μ_{ha} were the same for the 2 species, then the ratio of the areas of the bands would give R. However, the transition dipoles are not the same, and the areas of these bands are proportional to $C_{hw}\mu_{hw}^2$ and $C_{ha}\mu_{ha}^2$, where the Cs are the concentrations. The volumes of the *hw* band and the *ha* band on the diagonal of the 2D IR spectrum (see Fig. 2) are proportional to $C_{hw}\mu_{hw}^4$ and $C_{ha}\mu_{ha}^4$, respectively. The method for the determination of the volumes is discussed below. Combining the 2 types of measurements yields R and the ratio of the square of the transition dipoles. Within experimental error, we find that $R = 0.3$, the same as determined from the X-ray experiments (32), and $\mu_{hw}^2/\mu_{ha}^2 = 1.7$.

Fig. 1 displays the OD stretch spectrum of HOD in water and with increasing concentrations of $NaBF_4$. The value of n in Fig. 1 denotes the number of water molecules per molecule of $NaBF_4$. As the concentration of the salt increases, a peak develops on the high-frequency edge of the water spectrum. Its peak position is independent of concentration. This peak is attributed to ODs bonded to the BF_4^- anions (16). In addition, the water peak shifts to the blue with increasing concentration but essentially maintains its shape. At the concentration used in the CES experiments, 5.5 M, the shift is 19 cm^{-1}. At this high concentration, there is no bulk water in the sample. By bulk water, we mean water that is many solvent shells from an ion. At 5.5 M, which is 7 water molecules per $NaBF_4$, all of the water molecules will be associated with a cation, an anion, or both. At the highest concentration, fitting the 2 bands gives the peak positions and widths, which are: 2,526 cm^{-1} (165 cm^{-1}) and 2,646 cm^{-1} (45 cm^{-1}), where the number in parentheses is the full width at half maximum.

Fig. 2 displays contour plots of 2D IR vibrational echo data at $T_w = 200$ fs, which is short compared with the chemical exchange time. For clarity, the contours occur at intervals of 10% of the maximum. The data used in the analysis has much finer gradations. There are 4 bands, 2 going in the positive direction (labeled +) and 2 going in the negative direction (labeled −). The narrow positive peak to the upper right labeled ha_{01} arises from the *ha* 0–1 transition. Almost directly below it is the peak going in the negative direction produced by vibrational echo emission at the 1–2 transition of *ha*, labeled ha_{12}. This peak is slightly displaced to the right because of a small amount of overlap with the broad *hw* 0–1 transition going in the positive direction. The difference in the center frequencies of the *ha* 0–1 and 1–2 bands along the ω_m axis (vertical axis) is the anharmonic shift of the OD hydroxyl stretch for hydroxyls bound to anions. The shift is 90 cm^{-1}. Below the broad 0–1 *hw* band going in the positive direction (labeled hw_{01}) is the corresponding broad band going in the negative direction for the 1–2 transition of the OD *hw* stretch labeled hw_{12}. The anharmonic shift is 140 cm^{-1}.

Chemical exchange will cause 4 additional off-diagonal peaks to grow in, 2 of which are going in the positive direction, arising from the 0–1 diagonal transitions, and 2 that are going in the negative direction and come from the 1–2 transitions. Fig. 3*a* displays the 2D spectrum at $T_w = 4$ ps in which the growth of the chemical exchange peaks is clear. Only the higher–frequency region of the 2D spectrum is presented, making it easier to see the nature of the data. This portion of the spectrum is the part used in the data analysis discussed below. The IR pulses used in the experiments have a center frequency of 2,550 cm^{-1} to efficiently pump the 0–1 transition of *hw* and *ha*. The laser intensity is relatively weak in the *hw* 1–2 region, reducing the data quality at long times. In Fig. 3*a*, the exchange peaks are clearly visible. The most evident chemical exchange peak is the 0–1 $hw \rightarrow ha$ peak, labeled A in Fig. 3*a*. The spectrum shown in Fig. 3*a* contains 2 other exchange peaks. The 1–2 $hw \rightarrow ha$ peak is labeled B. Because the 1–2 $hw \rightarrow ha$ peak is negative, relatively narrow along the ω_m axis and extended along the ω_τ axis, it eats away a strip from the diagonal 0–1 *hw* band. This is seen very clearly by comparing the *hw* peak in Fig. 3*a* to its short-time counterpart in Fig. 2. The last exchange peak in Fig. 3*a* is the 0–1 $ha \rightarrow hw$ peak, labeled C. Like peak A, it is going in the positive direction and is manifested as a reduction in the bottom portion of the 1–2 *ha* peak going in the negative direction. The shapes of the diagonal and off-diagonal CES peaks have been explicated theoretically and experimentally (27, 38).

As discussed above, spectral diffusion causes the shapes of the bands to change with increasing T_w, but spectral diffusion does not change the peak volumes (27). Therefore, to determine the $hw \leftrightarrow ha$ chemical exchange rate, the peak volumes of the 6 peaks that occur in data like that presented in Fig. 3*a* are determined for a series of T_ws. A detailed theoretical study in which CES data were analyzed by using a full diagrammatic perturbation theory of the spectral diffusion (27) in addition to chemical exchange gave the same results as the method of fitting the peak volumes (25). The peaks are fit simultaneously with 6 2D Gaussian functions. The positions, widths, volumes, and tilts of the Gaussians are varied to minimize the square of the residuals. Although there are many parameters, there are also many constraints. For example, the diagonal 0–1 *ha* peak and the off-diagonal 1–2 *ha* peak should be identical in volume except for sign (positive vs. negative) and the shift along the ω_m axis, and

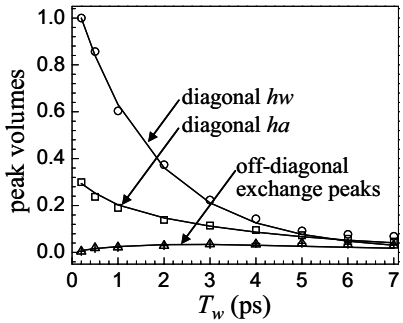

Fig. 4. Peak volumes as a function of T_w of the diagonal and chemical exchange peaks from data like those shown in Fig. 3. The solid curves are the result of to the exchange kinetic model.

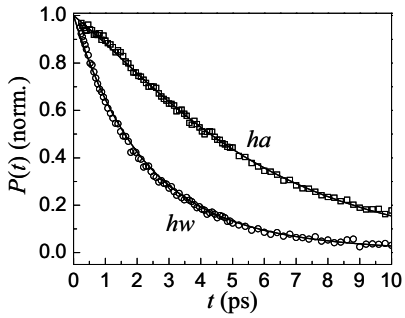

Fig. 5. Vibrational population decays for *ha* and *hw*. The solid curves are the result of simultaneously fitting the population decays and the peak volumes shown in Fig. 4 to the exchange kinetic model. The model accurately reproduces the highly nonexponential shape of the *ha* data.

the off-diagonal chemical exchange 0–1 $hw \rightarrow ha$ peak should be identical to the off-diagonal chemical exchange 0–1 $ha \rightarrow hw$ peak. In practice, experimental error results in such constraints not being met perfectly, but any serious deviation is an indication that the fit has settled into a false minimum. Fig. 3*b* is the result of fitting the data in Fig. 3*a*. It is clear that the fitting model reproduces the data with substantial accuracy.

Once the peak volumes are obtained for the series of 2D spectra over a range of T_w, it is necessary to relate the volumes to populations. The populations associated with the diagonal 0–1 *hw* and *ha* peaks are proportional to their volumes times μ_{hw}^4 and μ_{ha}^4, respectively. Assuming the harmonic approximation, the off-diagonal 1–2 *ha* peak also scales by μ_{ha}^4. The 3 off-diagonal chemical exchange peaks in Fig. 3 all scale as $\mu_{hw}^2\mu_{ha}^2$. The peak volumes are scaled by these factors by using the factor $\mu_{hw}^2/\mu_{ha}^2 = 1.7$, which was determined as described above. The time dependence of the *ha* 0–1 and 1–2 peaks should be the same (25, 27). The time dependence of all 3 chemical exchange off-diagonal peaks should be the same (25, 27). Therefore, all of the dynamics are reflected in the subset of peaks, the diagonal 0–1 *ha* peak, the diagonal 0–1 *hw* peak, and the off-diagonal 0–1 chemical exchange $hw \rightarrow ha$ peak. These are plotted in Fig. 4. The data are normalized to the shortest time point of the *hw* peak.

To obtain the chemical exchange rate, it is necessary to fit the data in Fig. 4 with a model that includes the vibrational population decay rates of *hw* and *ha*, and the orientational relaxation rates of *hw* and *ha*. In analyzing the data, the procedures applied previously are used (25, 27). However, there are 2 complications. In earlier experiments on, for example, the formation and dissociation of phenol-benzene π hydrogen bonded solute–solvent complexes in the mixed solvent of benzene and carbon tetrachloride (25), it was possible to make independent determinations of the population and orientational decay rates. In the current experiments, it is not possible to make the equivalent measurements, so the exchange data and measured vibrational lifetime decays are fit simultaneously by using the same kinetic model. The advantage of this fitting method is that it provides an internally consistent confirmation that the 2 very different types of measurements provide the same information about the underlying molecular dynamics of the system.

Polarization selective pump-probe experiments were used to determine the apparent lifetime and orientational relaxation rate for *ha* at the frequency of the 0–1 transition of *ha*, 2,646 cm^{-1}. The apparent lifetime and orientational relaxation rate for *hw* were determined at the frequency of the 1–2 transition of *hw*, 2,365 cm^{-1}, rather than at the 0–1 transition, because the 1–2 transition of *ha* overlaps with the 0–1 transition of *hw*. By using the equilibrium constant *R* and the measured values as an initial guess, the data in Figs. 4 and 5 were simultaneously fit to a system of coupled differential equations (27). In the fitting, the only adjustable parameters are the 2 vibrational lifetimes and the exchange rate for the process, $ha \rightarrow hw$. To reduce the number of adjustable parameters, the orientational times were not varied in the fitting because, as discussed below, the time scale for reorientation is almost the same for the 2 species, so exchange has very little effect on the measured values. It was found that if the exchange data in Fig. 4 were fit with the $ha \rightarrow hw$ exchange rate as a single adjustable parameter by using an initial guess for the lifetimes as fixed input parameters, the resulting exchange rate was fairly close to the value found from the simultaneous fits, but the quality of the fits was not nearly as good. The simultaneous fitting is necessary to obtain the correct vibrational lifetimes and correct functional forms of the population decays as well as to obtain high quality fits through all 3 datasets in Fig. 4. The simultaneous fits give an exchange rate, vibrational lifetimes, and orientational relaxation times that are internally consistent with the data measured by 2D IR CES and polarization selective pump-probe spectroscopy.

The fits to the exchange model are shown as the solid curves in Figs. 4 and 5. The quality of the fits in both Figures is excellent. In Fig. 4, the fit reproduces the time dependence of the diagonal and chemical exchange peaks. The exchange time for $ha \rightarrow hw$ is $T_{aw} = 7 \pm 1$ ps. The exchange time for $hw \rightarrow ha$, T_{wa}, is related to T_{aw} by the equilibrium constant. Because the system is in equilibrium, $R = k_{wa}/k_{aw}$, where $k_{aw} = 1/T_{aw}$ and $k_{wa} = 1/T_{wa}$ are the rate constants for exchange and *R* is the equilibrium constant. Using $R = 0.3$ gives $T_{wa} = 24$ ps. This value will be dependent on the concentration of salt because $hw \rightarrow ha$ can only occur if a water molecule is very close to an anion. Therefore, the exchange dynamics are better characterized by the time constant, $T_{aw} = 7$ ps, which may be relatively insensitive to salt concentration as discussed below.

Fig. 5 shows the vibrational population relaxation for *hw* and *ha* with the results of the exchange model fit as solid curves. The process of exchange modifies the vibrational population decays such that the experimentally measured decays do not provide the true lifetimes. Initially, the data are fit with single exponential decays to extract a first guess for the lifetimes. The *hw* decay is substantially faster than the *ha* decay. Because the system is in equilibrium, at $t = 0$, equal population is exchanged between the 2 species. However, as time proceeds, the *hw* population decays more than the *ha* population, and the exchange process will serve to bolster the population of *hw*, making the apparent lifetime longer than the true lifetime. The converse is true for *ha*. As discussed below, the shapes of the population decay curves, particularly the *ha* curve, are substantially influenced by the chemical exchange. Note that the number of molecules undergoing exchange is always constant, but the fraction of excited molecules of each species depends on the vibrational lifetime of that species.

The *hw* decay is close to exponential because the intrinsic lifetime is much shorter than the exchange time. A single exponential fit to the *hw* population decay gives the apparent time constant, $\tilde{\tau}_{hw} = 2.5$ ps. The tilde indicates an apparent lifetime. However, the *ha* decay is far from exponential, and it is remarkable how well the exchange model reproduces its nonexponential shape. At early times, before significant exchange has occurred, the *ha* population decay is fairly close to the true lifetime. A single exponential fit to the *ha* lifetime decay from 0.2 ps to 2 ps gives a time constant of $\tilde{\tau}_{ha} = 8$ ps. In Fig. 5, it can be seen that the *ha* decay during the first picosecond is slower and then becomes steeper as the exchange process shortens the apparent vibrational lifetime. A fit beginning at 3 ps (after exchange has begun to play a role) gives an apparent time constant of $\tilde{\tau}_{ha} = 4.7$ ps. Simultaneously fitting the 2D IR CES data and the pump probe data yields the true values for the lifetimes of $\tau_{hw} = 2.2 \pm 0.1$ ps and $\tau_{ha} = 9.4 \pm 1$ ps. The true values are consistent with the exchange process increasing the apparent lifetime of the fast component and decreasing the apparent lifetime of the slow component.

Measurements of the anisotropy following procedures described previously (2) yields values of $\tau_r^{ha} = 5.0$ ps and $\tau_r^{hw} = 4.1$ ps where τ_r^{ha} and τ_r^{hw} are the long time orientational correlation times for *ha* and *hw*, respectively. The orientational dynamics of *ha* are biexponential with a fast component of 0.7 ps due to fast orientational motion within an intact hydrogen bonding configuration (39). The biexponential nature of the orientational dynamics of *ha* is well described by a wobbling-in-a-cone model (39–41), and its effects on the exchange process were included in the fitting described above. Because of space limitations, the orientational relaxation data are not shown here. Because the values for the long time components of the orientational relaxation are quite similar, they are changed negligibly by exchange.

The time constants for orientational motion are faster than the time constant for chemical exchange, $T_{aw} = 7 \pm 1$ ps. The orientational relaxation times and the chemical exchange times are not directly comparable because the orientational decay time is the decay of the second Legendre polynomial correlation function. Nonetheless, it is reasonable to expect that orientational relaxation will be faster than chemical exchange. In pure water, orientational relaxation is modeled as jump reorientation. Here, the jumps can be from *ha* to *hw* and *hw* to *ha*, as well as *ha* to *ha*, and *hw* to *hw*. The first 2 types of jumps produce both chemical exchange and orientational relaxation, whereas the last 2 produce only orientational relaxation. In addition, it has been proposed that the bonding of a water hydroxyl to BF_4^- is not spatially specific to the fluorines (42). Hydrogen bond rearrangements affecting the other hydroxyl might cause the *ha* to move on the surface of the anion, producing orientational relaxation. Thus, there are more pathways contributing to orientational relaxation than to chemical exchange, in accord with the observation of faster reorientation. Interestingly, the orientational relaxation times are less than a factor of 2 slower than the orientational relaxation time of pure water, $\tau_r = 2.6$ ps. Thus, the dynamics of water in this concentrated salt solution are not tremendously slower than in pure water.

Previously, 2D IR vibrational echo experiments and pump-probe experiments were used to study water dynamics in NaBr solutions at several concentrations (8, 41). It was found that the concentration dependence of the FFCF and the orientational relaxation were identical. These results and their agreement with MD simulations (43) were interpreted as reflecting the exchange time. However, in this earlier experimental study, the exchange was not measured directly, and the additional pathways that could lead to reorientation or spectral diffusion without exchange were not considered. In accord with the results reported here, the orientational relaxation times were slower than that of pure water but only by approximately a factor of 2. Based on the results obtained here, it is likely that the NaBr $ha \leftrightarrow hw$ exchange is somewhat slower than suggested previously (8, 41).

In the concentrated solution studied here, the solvation shells of the cations and anions are strongly overlapped, and it is quite possible that there is no second solvation shell of water molecules. It is important to note that a chemical exchange event does not require that a water molecule leaves the first solvation shell of the anion. All that is necessary for an exchange event to be observed is that a hydrogen bond rearrangement occurs so that $ha \rightarrow hw$ or $hw \rightarrow ha$. On a molecular level, this may occur if an HOD initially donating an OD hydrogen bond to BF_4^- undergoes an exchange event and ends up donating its OH hydrogen bond to the same BF_4^-. Although this mechanism has been observed in simulations of bulk water (44), it is much more common for the donating water molecule to move out of the first solvation shell of the initial acceptor (21, 22). The data reported here demonstrate that the time for hydrogen bond switching in this concentrated solution is slower than in bulk water, but only by a relatively small factor. If solvation shell exchange is governed by hydrogen bond switching, it is reasonable to expect that the exchange time reported here for $ha \rightarrow hw$, $T_{aw} = 7 \pm 1$ ps, is representative of the time scale for a water molecule to leave the solvation shell of an anion in more dilute solutions.

Two-color pump probe IR studies have suggested that the dynamics of water in the solvation shell of ions are substantially slower than in pure water (24). In contrast, NMR studies of water solvating ions (10, 18) and proteins (1) suggested that the dynamics are not drastically different from those of pure water. Recent MD simulations (21, 22) and ultrafast 2D IR experiments (8, 41) also suggest that water dynamical processes do not slow drastically in the proximity of ions. The current 2D IR CES experiments provide a direct measurement of the $hw \leftrightarrow ha$ chemical exchange. Combined with the pump-probe experiments and the application of the exchange model to the dynamics measured with both CES and pump-probe, significant details of water dynamics in the proximity of ions have been explicated.

Concluding Remarks

Chemical exchange in the solvation shells of BF_4^- in concentrated aqueous solutions of $NaBF_4$ was measured with a combination of 2D IR CES and polarization selective pump-probe spectroscopy. The exchange events consist of hydroxyls switching hydrogen bonding partners between BF_4^- anions (*ha*) and water oxygens (*hw*). A kinetic model, which includes the effects of the different vibrational lifetimes and orientational relaxation of the 2 species, was fit to the exchange data and pump probe data. The agreement between the model and the data (Figs. 4 and 5) is excellent and the time constant for chemical exchange, $ha \rightarrow hw$ is $T_{aw} = 7 \pm 1$ ps. The experiments show that the time scale for a hydroxyl to switch from being hydrogen bonded to an anion to being bonded to a water oxygen is only several times longer than the time scales for hydrogen bond rearrangement dynamics in pure water. These results have broad implications, suggesting a relatively short residence time for water near many charged solutes including the charged amino acids at the surfaces of proteins.

Materials and Methods

The CES experiments are performed on the OD hydroxyl stretch of dilute (5%) HOD in $H_2O/NaBF_4$ at 298 K. The concentration of $NaBF_4$ used in the CES experiments is 5.5 M. A Ti:Sapphire oscillator/regenerative amplifier pump an OPA and difference frequency stage to produce ≈70-fs IR pulses.

ACKNOWLEDGMENTS. This work was supported by Department of Energy Grant DE-FG03-84ER13251, National Institutes of Health Grant 2-R01-GM061137-09, and Air Force Office of Scientific Research Grant F49620-01-1-0018. D.E.M. thanks the National Science Foundation for a Graduate Research Fellowship. D.E.R. thanks the Fannie and John Hertz Foundation and a Stanford Graduate Fellowship program for graduate research fellowships.

1. Modig K, Liepinsh E, Otting G, Halle B (2004) Dynamics of protein and peptide hydration. *J Am Chem Soc* 126:102–114.
2. Moilanen DE, *et al.* (2008) Water inertial reorientation: Hydrogen bond strength and the angular potential. *Proc Natl Acad Sci USA* 105:5295–5300.
3. Asbury JB, *et al.* (2004) Water dynamics: Vibrational echo correlation spectroscopy and comparison to molecular dynamics simulations. *J Phys Chem A* 108:1107–1119.
4. Fecko CJ, Loparo JJ, Roberts ST, Tokmakoff A (2005) Local hydrogen bonding dynamics and collective reorganization in water: Ultrafast infrared spectroscopy of HOD/D_2O. *J Chem Phys* 122:054506–054518.
5. Rezus YLA, Bakker HJ (2005) On the orientational relaxation of HDO in liquid water. *J Chem Phys* 123:114502.
6. Laage D, Hynes JT (2006) A molecular jump mechanism of water reorientation. *Science* 311:832–835.
7. Asbury JB, *et al.* (2004) Dynamics of water probed with vibrational echo correlation spectroscopy. *J Chem Phys* 121:12431–12446.
8. Park S, Fayer MD (2007) Hydrogen bond dynamics in aqueous NaBr solutions. *Proc Natl Acad Sci USA* 104:16731–16738.
9. Ohtaki H, Radnai T (1993) Structure and dynamics of hydrated ions. *Chem Rev (Washington, DC)* 93:157–1204.
10. Endom L, Hertz HG, Thül B, Zeidler MD (1967) A microdynamic model of electrolyte solutions as derived from nuclear magnetic relaxation and self-diffusion data. *Ber Bunsenges Phys Chem* 71:1008–1031.
11. Marcus Y (1985) *Ion Solvation* (Wiley, New York).
12. Bagchi B (2005) Water dynamics in the hydration layer around proteins and micelles. *Chem Rev* 105:3197–3219.
13. Corcelli S, Skinner JL (2005) Infrared and raman line shapes of dilute hod in liquid H_2O and D_2O from 10 to 90 °C. *J Phys Chem A* 109:6154–6165.
14. Falk M, Ford TA (1966) Infrared spectrum and structure of liquid water. *Can J Chem* 44:1699.
15. Bergström P-A, Lindgren J, Kristiansson O (1991) An IR study of the hydration of ClO_4^-, NO_3^-, I^-, Br^-, Cl^-, and SO_4^{2-} anions in aqueous solution. *J Phys Chem* 95:8575–8580.
16. Brink G, Falk M (1970) Infrared spectrum of HDO in aqueous solutions of perchlorates and tetrafluoroborates. *Can J Chem* 48:3019–3025.
17. Kropman MF, Bakker HJ (2003) Vibrational relaxation of liquid water in ionic solvation shells. *Chem Phys Lett* 370:741–746.
18. Shimizu A, Taniguchi Y (1991) NMR studies of reorientational motion of hydrated D_2O molecules of halide ions (F^-, Cl^-, Br^-, and I^-) in dilute aqueous solutions. *Bull Chem Soc Jpn* 64:1613–1617.
19. Mancinelli R, Botti A, Bruni F, Ricci MA, Soper AK (2007) Hydration of sodium, potassium, and chloride ions in solution and the concept of structure maker/breaker. *J Phys Chem B* 111:13570–13577.
20. Heuft JM, Meijer EJ (2003) Density functional theory based molecular-dynamics study of aqueous chloride solvation. *J Chem Phys* 119:11788–11791.
21. Laage D, Hynes JT (2007) Reorientational dynamics of water molecules in anionic hydration shells. *Proc Nat Acad Sci* 104:11167–11172.
22. Laage D, Hynes JT (2008) On the residence time for water in a solute hydration shell: Application to aqueous halide solutions. *J Phys Chem B* 112:7697–7701.
23. Smith JD, Saykally RJ, Geissler PL (2007) The effect of dissolved halide anions on hydrogen bonding in liquid water. *J Am Chem Soc* 129:13847–13856.
24. Kropman MF, Bakker HJ (2001) Dynamics of water molecules in aqueous solvation shells. *Science* 291:2118–2120.
25. Zheng J, *et al.* (2005) Ultrafast dynamics of solute–solvent complexation observed at thermal equilibrium in real time. *Science* 309:1338–1343.
26. Kim YS, Hochstrasser RM (2005) Chemical exchange 2D IR of hydrogen-bond making and breaking. *Proc Natl Acad Sci* 102:11185–11190.
27. Kwak K, Zheng J, Cang H, Fayer MD (2006) Ultrafast 2D IR vibrational echo chemical exchange experiments and theory. *J Phys Chem B* 110:19998–20013.
28. Zheng J, Kwak K, Chen X, Asbury JB, Fayer MD (2006) Formation and dissociation of intraintermolecular hydrogen bonded solute–solvent complexes: Chemical exchange 2D IR vibrational echo spectroscopy. *J Am Chem Soc* 128:2977–2987.
29. Zheng J, Kwak K, Xie J, Fayer MD (2006) Ultrafast carbon-carbon single bond rotational isomerization in room temperature solution. *Science* 1951–1955.
30. Kwak K, Rosenfeld DE, Chung JK, Fayer MD (2008) Solute–solvent complex switching dynamics of chloroform between acetone and dimethylsulfoxide two-dimensional IR chemical exchange spectroscopy. *J Phys Chem B* 112:13906–13915.
31. Ishikawa H, Kwak K, Chung JK, Kim S, Fayer MD (2008) Direct observation of fast protein conformational switching. *Proc Natl Acad Sci USA* 105:8619–8624.
32. Ryss AI, Radchenko IV (1964) An X-ray diffraction study of aqueous sodium tetrafluoroborate solutions. *Zhurnal Strukturnoi Khimii* 5:530–533.
33. Woutersen S, Bakker HJ (1999) Resonant intermolecular transfer of vibrational energy in liquid water. *Nature (London)* 402:507–509.
34. Gaffney KJ, Piletic IR, Fayer MD (2003) Orientational relaxation and vibrational excitation transfer in methanol–carbon tetrachloride solutions. *J Chem Phys* 118:2270–2278.
35. Gochanour CR, Fayer MD (1981) Electronic excited state transport in random systems: Time resolved fluorescence depolarization measurements. *J Phys Chem* 85:1989–1994.
36. Corcelli S, Lawrence CP, Skinner JL (2004) Combined electronic structure/molecular dynamics approach for ultrafast infrared spectroscopy of dilute hod in liquid H_2O and D_2O. *J Chem Phys* 120:8107.
37. Park S, Kwak K, Fayer MD (2007) Ultrafast 2D IR vibrational echo spectroscopy: A probe of molecular dynamics. *Laser Phys Lett* 4:704–718.
38. Zheng J, Fayer MD (2008) Solute–solvent complex kinetics and thermodynamics probe by 2D IR vibrational echo chemical exchange spectroscopy. *J Phys Chem B* 112:10221–10227.
39. Moilanen DE, Piletic IR, Fayer MD (2007) Water dynamics in nafion fuel cell membranes: The effects of confinement and structural changes on the hydrogen bonding network. *J Phys Chem C* 111:8884–8891.
40. Lipari G, Szabo A (1982) Model-free approach to the interpretation of nuclear magnetic-resonance relaxation in macromolecules. 1. Theory and range of validity. *J Am Chem Soc* 104:4546–4559.
41. Park S, Moilanen DE, Fayer MD (2008) Water dynamics-the effects of ions and nanoconfinement. *J Phys Chem B* 112:5279–5290.
42. Akitt JW (1975) Multinuclear nuclear magnetic-resonance studies of aqueous-solutions of tetrafluoroborate salts. *J Chem Soc Faraday Transact I* 71:1557–1572.
43. Chowdhuri S, Chandra A (2006) Dynamics of halide ion–water hydrogen bonds in aqueous solutions: Dependence on ion size and temperature. *J Phys Chem B* 110:9674–9680.
44. Laage D, Hynes JT (2008) On the molecular mechanism of water reorientation. *J Phys Chem B* 112:14230–14242.